Heliyon 10 (2024) e31716

Contents lists available at ScienceDirect

Heliyon

journal homepage: www.cell.com/heliyon

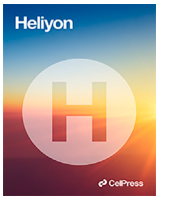

Research article

An intelligent climate monitoring system for hygrothermal virtual measurement in closed buildings using Internet-of-things and artificial hydrocarbon networks

Hiram Ponce [a,*], Sebastián Gutiérrez [b], Juan Botero-Valencia [c], David Marquez-Viloria [c], Luis Castano-Londono [d]

[a] Universidad Panamericana, Facultad de Ingeniería, Augusto Rodin 498, Ciudad de México, 03920, Mexico
[b] TECNUN Escuela de Ingeniería, Universidad de Navarra, Manuel Lardizabal 13, San Sebastián, 20018, Spain
[c] Facultad de Ingenierías, Instituto Tecnológico Metropolitano, Calle 73 No. 76A-354, Medellin, 050034, Colombia
[d] Facultad de Ingeniería, Universidad de Antioquia, Calle 70 No. 52-21, Medellin, 050010, Colombia

ARTICLE INFO

Keywords:
Artificial hydrocarbon networks
Failure detection
Internet-of-things
Machine learning

ABSTRACT

Studies analyzing indoor thermal environments comprising temperature and humidity may be insufficient when obtaining data from sensors, which may be susceptible to inaccurate or failed information from internal and external factors. Therefore, this study proposes an intelligent climate monitoring using a supervised learning method for virtual hygrothermal measurement in enclosed buildings used to predict temperature and relative humidity when a sensor failure is detected. The methodology comprises the data collection from a wireless sensor network, the building of the learning model for predicting the dynamics of environmental variables, and the implementation of a sensor failure detection model. We use an artificial hydrocarbon network as the learning model for their simplicity and effectiveness under uncertain and noisy data. The experiments use data acquired in two settings: (1) a laboratory office and (2) a museum storage room. The first scenario has multiple workstations, and the staff turns on or off the air conditioning depending on the feeling of comfort, generating an uncontrolled environment for the variables of interest. The second scenario has controlled temperature and humidity to ensure the conservation conditions of the museum pieces. Both scenarios used 12 sensors that acquired data for one month, providing an average of 58,300 values for each variable. Results of the proposed methodology provide 95% of accuracy in terms of sensor failure detection and identification, and less than 0.22% of tolerance variability in temperature and humidity after sensor accommodation in both scenarios.

1. Introduction

Thermal comfort in buildings is important for human well-being because people spend approximately 90% of their time indoors [1]. Inadequate environmental conditions, such as increased temperature and humidity, can directly affect the health of the occupants

* Corresponding author.
E-mail addresses: hponce@up.edu.mx (H. Ponce), jsgutierrez@tecnun.es (S. Gutiérrez), juanbotero@itm.edu.co (J. Botero-Valencia), davidmarquez@itm.edu.co (D. Marquez-Viloria), luis.castanol@udea.edu.co (L. Castano-Londono).

https://doi.org/10.1016/j.heliyon.2024.e31716
Received 3 February 2024; Received in revised form 30 April 2024; Accepted 21 May 2024

Available online 23 May 2024

by promoting conditions for the transmission of bacteria, viruses, and respiratory infections [2] [3]. Moreover, humidity inside buildings significantly affects the comfort and health of the occupants and energy consumption [4].

In recent years, maintaining individual occupants' comfort has attracted substantial interest in smart building control systems. Indoor temperature and humidity control systems use a wide range of techniques to ensure thermal comfort for people or the proper preservation of historically significant pieces. Those systems adopted thermal comfort standards such as ASHRAE 55 and ISO 7730 [5]. Previous works have revealed the relationship of many correlated parameters to predict an individual's thermal comfort level for personal comfort optimization purposes [6] [7]. Additionally, a recent study [8] introduces a classification of thermal environment control indicators based on the thermal sensitivity of office occupants. This study proposes control indicators and tailored guidelines for groups categorized by their thermal sensitivity, potentially influencing the design and operation of office buildings to enhance thermal comfort.

Some studies have also indicated that using sensors and actuators for climate control inside buildings aims to reduce energy consumption and improve the conditions of the occupants [9]. For this reason, researchers are interested in using machine learning algorithms to develop data-driven models for predicting the thermal sensation of occupants [10] and building energy efficiency [11]. A systematic review of data-driven approaches for predicting thermal comfort in a building environment is presented in [5], considering experimental design, data collection, and model techniques.

As part of hygrothermal analysis [2], the measurement of temperature and humidity in closed environments has been extensively studied [12]. It is generally associated with indoor air quality monitoring systems, in which particulate matter and different types of gases present in the environment are measured. Works like those presented in [12,13] present monitoring systems in housing environments in which data acquisition is performed using sensor networks to study indoor environmental conditions. Different studies can be found that perform data acquisition using low-cost devices and Internet of Things (IoT) technology. Some IoT-based monitoring systems are described in the literature in [14–16].

Systems based on IoT that contain many sensors continue to produce a large amount of data, which, at the time of transmission, may fail due to environmental interference [17] and aging or the quality of the devices [18,19]. In [20] is presented a survey on fault detection in wireless sensor networks (WSN), in which the authors identify three approaches for failure detection in wireless sensor networks: centralized, distributed, and hybrid. The WSNs feed the systems in charge of controlling the actuators and the different building systems to maintain the desired comfort measures. However, the control techniques depend on the reliability of the measurements they are receiving from the sensors.

Buildings are large systems that need the deployment of sensor networks that feed the different systems, such as heating, air conditioning, ventilation, and lighting. Some researches propose the integration of virtual sensors to increase redundancy in the systems to support the decision-making of control algorithms and fault detection [21–23]. Virtual sensors are generated using information from physical sensors. The number of sensors and the geographical location can be determined by methodologies that optimize the resources in the sensor network [24]. Because of this, modern systems should include sensor fault detection, identification, and accommodation (SFDIA) to avoid the adverse effects that sensor failure can cause. In [25], a method for SFDIA in HVAC systems is presented using a soft-sensor approach. The goal is to improve system reliability by accurately detecting, identifying, and accommodating sensor faults. Even fast response systems such as an unmanned air vehicle (UAV) can combine the control system and SFDIA using machine learning techniques such as neural networks [26,27].

In recent works, a machine learning method namely artificial hydrocarbon networks (AHN) has been proposed [28]. This is a supervised learning method inspired by the structures and mechanisms of organic molecules, aiming to model and structure data in packages of information. AHN has been widely explored in intelligent control systems [29], robotics [30], sensor signals [31, 32], biomedical and health applications [33,34], among others [28,35], proving their effectiveness in both performance and low computational resources. Thus, we consider AHN might be a good machine learning candidate for SFDIA systems.

This paper proposes an intelligent climate monitoring based on AHN that can act as a SFDIA system over a WSN in real-time, for hygrothermal analysis. The intelligent climate monitoring consists of a set of sensor nodes that are connected wirelessly using IoT. These nodes report climate variables, i.e. temperature and humidity, of different locations of indoor buildings. A server in the WSN processes the information from the sensors, and the SFDIA based on AHN models can detect possible sensor failure, identifying the source node of the corrupted signals, and replacing the sensor signals with accommodated signals estimated by the SFDIA system, while the failure persists. The accommodated signals are then use for hygrothermal analysis. We implement our intelligent climate monitoring in two case scenarios: (Scenario 1) a laboratory office with staff for thermal comfort testing, and (Scenario 2) a museum storage room with specimens and collectibles. In Scenario 1, the room has people inhabiting the space under uncontrolled temperature and humidity conditions. Scenario 2 has no permanent people inside the area and has controlled temperature and humidity conditions. After one month of experimentation in each scenario, the results of our intelligent climate monitoring include that it detects and identifies sensor failures with 95% of accuracy, and it accommodates sensor signals with root mean squared errors less than 0.22 RH% in humidity and 0.08 ºC in temperature.

The main contributions of this work include:

- A novel intelligent climate monitoring system using AHN for hygrothermal analysis in indoor buildings. It is a SFDIA approach over a WSN in real-time that consists of a set of sensor nodes connected wirelessly using IoT.
- To detect possible sensor failure, identify the source node of the corrupted signals, and replace the sensor signals with estimates, AHN models capture dynamic changes in sensor nodes.
- The AHN models and the adaptive WSN implemented allow the intelligent climate monitoring system to be flexible to different measurement variables, i.e. humidity or temperature, and different number of sensor nodes.

The rest of the paper is organized as follows. Section 2 describes our proposed intelligent climate monitoring system. Section 3 presents two case scenarios where the proposed system was implemented. Section 4 presents experimental results. Section 5 describes the influence of the proposed SFDIA system in hygrothermal analysis. Section 6 presents a discussion of the proposal, and Section 7 concludes this work.

2. Intelligent climate monitoring

In this work, we propose an intelligent climate monitoring that can act as a sensor failure detection, identification, and accommodation system (SFDIA) over a wireless sensor network (WSN) in real-time, for hygrothermal analysis.

2.1. Artificial hydrocarbon networks

The core of the intelligent climate monitoring is a machine learning-based model using artificial hydrocarbon networks (AHN), a supervised learning method inspired by the structure of organic molecules [28]. The method consists of representing data as a net of structured entities called molecules. The network, as shown in Fig. 1, captures the nonlinearities of the inputs into the molecules and, then, outputs the responses as a combination of the molecular behaviors so-called compounds. Several compounds can mix together to form a mixture. As noticed, an AHN model considers a different conception of the structure. It is organized in levels of complexity, from the less complex (molecules), middle complex (compounds) to the most complex (mixture), and it differs from traditional layer-based models such as neural networks. In this work, we only consider a mixture with one compound made up of a set of molecules [28].

In this method, an AHN molecule consists of one carbon atom and k hydrogen atoms linked to it, written as CH_k $(1 < k \leq 4)$. The output of the molecule, denoted as $\varphi(x)$, is shown in (1); where, $\sigma \in \mathbb{R}^n$ represents the carbon value, $H_i \in \mathbb{R}^n$ corresponds to the ith hydrogen value (attached to the carbon), and $x = (x_1, \ldots, x_n)$ is the input vector with n features.

$$\varphi(x;k) = \sum_{r=1}^{n} \sigma_r \prod_{i=1}^{k\leq 4} (x_r - H_{i,r}) \tag{1}$$

An AHN compound is a structure formed by the interaction of two or more molecules, each having up to three hydrogen atoms attached. For simplicity, in this work, we adopt a compound that consists of a sequence of molecules: two CH_3 molecules at the extremes and $(m-2)$ CH_2 molecules in the middle [28]. The output of a compound is represented by the function $\psi(x)$ as shown in (2). Here, φ_j represents the output of the jth molecule that clusters a subset Σ_j of the input vector x, defined as $\Sigma_j = \{x | \arg\min_j (x - \mu_j) = j\}$, where $\mu_j \in \mathbb{R}^n$ represents the center of the jth molecule. Then, it is important to ensure non-overlapping subsets.

$$\psi(x) = \begin{cases} \varphi_1(x,3) & x \in \Sigma_1 \\ \varphi_2(x,2) & x \in \Sigma_2 \\ \cdots & \cdots \\ \varphi_{m-1}(x,2) & x \in \Sigma_{m-1} \\ \varphi_m(x,3) & x \in \Sigma_m \end{cases} \tag{2}$$

An AHN mixture represents high-level units of information, consisting of a linear combination of a set of compounds, as denoted in (3). Here, α_i are weights for compounds, and C is the total number of compounds in the mixture.

$$S(x) = \sum_{i}^{C} \alpha_i \varphi_i(x) \tag{3}$$

To build an AHN model, it requires two hyperparameters: the number of molecules m in the compound and the batch size $0 < b \leq 1$ that is the percentage of training data randomly chosen by the training algorithm each iteration. Literature reports several training procedures, but we use the stochastic parallel extreme (SPE-AHN) training algorithm [28] to compute the learning parameters, denoted as ω. For more details about AHN, we refer the reader to the following references [28,29].

2.2. Architecture of the intelligent climate monitoring

The intelligent climate monitoring is over a WSN in which a set of sensor nodes measure the climate variables (e.g., temperature and humidity). These sensor nodes communicate the measurements to the gateway that collects and transmits all data to a server in which the SFDIA system is executed. If a sensor failure is detected, the system identifies the corrupted sensor and replaces the corrupted signal (accommodation) with value estimations of the climate variables while the failure persists. Lastly, the intelligent climate monitoring presents the sensing variables, or the accommodation signals, to the user so that a hygrothermal analysis can be conducted. The overall system is depicted in Fig. 2.

The SFDIA system of the intelligent climate monitoring consists of four modules, as shown in Fig. 3: sensor failure detection module (Section 2.2.1), sensor identification module (Section 2.2.2), sensor accommodation module (Section 2.2.3), and online

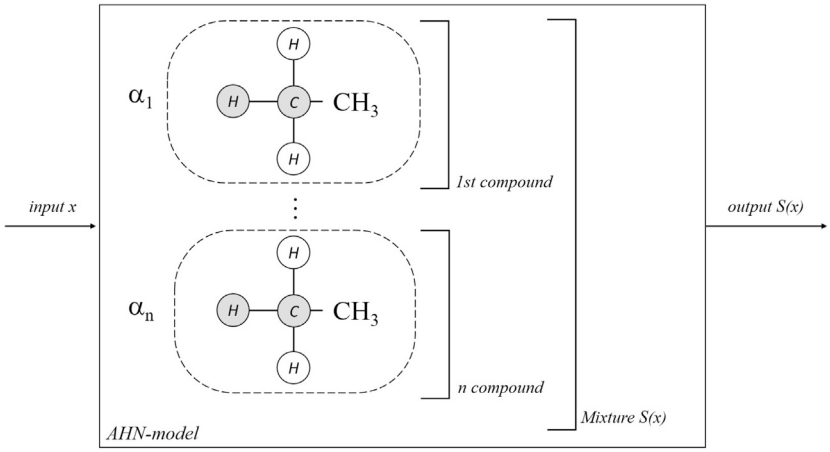

Fig. 1. Simple representation of an artificial hydrocarbon network model.

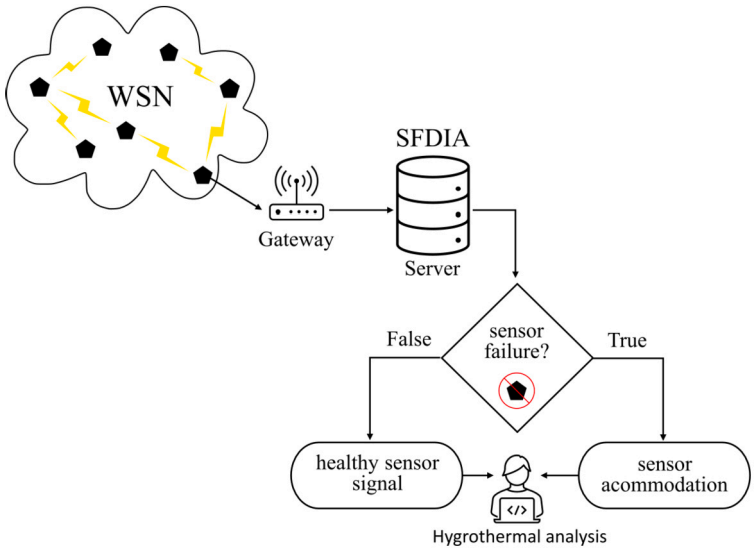

Fig. 2. Intelligent climate monitoring: The WSN transmits all data to a server where the SFDIA system is executed. In case of sensor failure, the system identifies and replaces the corrupted signal. Accommodation signals are then presented to conduct hygrothermal analysis.

statistics module (Section 2.2.4). Internally, the system needs to train different AHN models and update a few required statistics, as detailed next.

2.2.1. *Sensor failure detection module*

The first step of the SFDIA system is to detect failures in the sensor nodes due to environment noise, communication loss, data buffer fullness, node stoppage, etc., such that the climate signals are corrupted over a period of time. To do so, we develop a sensor failure module by taking into account the information across the sensors over time. The key idea behind this module is to detect an abnormal change between the actual measurements of the sensor nodes and the estimates of the signals of the climate variables in dependence on each other using a dynamic model.

The system consists of k sensor nodes, $N = \{n_1, \ldots, n_k\}$. We consider the dynamic model $f^{(i)}_{AHN}$ of the sensor signals, related to node i, to be (4); where n_i represents the sensor signal of node i, $n_{\setminus i}$ represents the set of sensor signals except the one from node i, $\Delta n_{\setminus i}$ is the change of the sensor signals $n_{\setminus i}$, and t is the time.

$$\Delta n_{\setminus i}(t+1) = f^{(i)}_{AHN}\left(n_i(t), n_{\setminus i}(t)\right) \tag{4}$$

We propose the dynamic model $f^{(i)}_{AHN}$ to be an AHN model that is trained using the input pair $x_j = \{n_i(t-1), n_{\setminus i}(t-1)\}$ and the output difference $o_j = \{n_{\setminus i}(t) - n_{\setminus i}(t-1)\}$, for all samples $j = 1, \cdots, T$ in the time series of length T. For training, we use the loss function $\mathcal{L}_f(\omega)$ shown in (5), where ω represents the learning parameters of AHN. It is remarkable to say that the training data must be healthy data (i.e., without corrupted sensor signals).

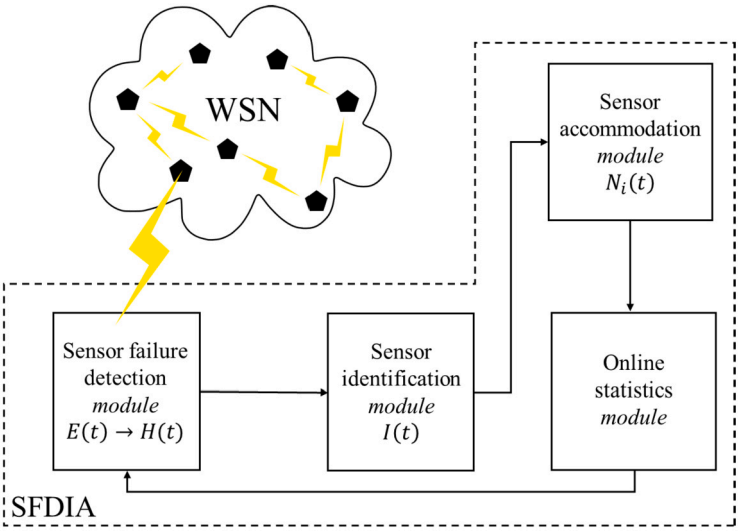

Fig. 3. SFDIA system of the intelligent climate monitoring. Four steps are performed: the sensor failure detection module identifies possible failures in the WSN, the sensor identification module determines which sensor has failed, the sensor accommodation module replaces the corrupted sensor signal with a proper value, and the online statistics module updates the failure detection function over a given period of time.

$$\mathcal{L}_f(\omega) = \frac{1}{2}\sum_j \left(o_j - f^{(i)}_{AHN}(x_j|\omega)\right)^2 \tag{5}$$

Accordingly to (4) and the definition of the training outputs of the AHN model, it is possible to estimate the sensor signals of the WSN, related to node i, denoted by $\hat{n}_{\setminus i}$, as written in (6). As noticed, this estimation depends on the sensor signal n_i. It can be used to detect possible failures in the WSN if the difference between the estimates and the actual sensor signals is large. For a global impact of these changes, we can compute the total difference E as shown in (7). Lastly, we propose a failure detection function H like (8) that computes if the standardized total difference E is greater than a threshold value α, where μ and σ are the mean and standard deviation of E over a given period of time, as further described in Section 2.2.4.

$$\hat{n}_{\setminus i}(t) = n_{\setminus i}(t-1) + f^{(i)}_{AHN}\left(n_i(t-1), n_{\setminus i}(t-1)\right) \tag{6}$$

$$E(t) = \sum_{i=1}^{k} \|n_{\setminus i}(t) - \hat{n}_{\setminus i}(t)\| \tag{7}$$

$$H(t) = \begin{cases} 1 & \frac{E(t)-\mu}{\sigma} > \alpha \\ 0 & otherwise \end{cases} \tag{8}$$

2.2.2. Sensor identification module

Once a sensor failure is detected by H, the next step of the SFDIA system is to identify the sensor that failed. We propose a dynamic model $g^{(i)}_{AHN}$ of the sensor signal of node i to be (9). As noticed, this model estimates the sensor signal of node i, denoted as $\hat{n}_i(t)$, by considering the actual and past states of the sensor signals except the one from node i. The dynamic model $g^{(i)}_{AHN}$ is trained using the input pair $x_j = \{n_{\setminus i}(t), n_{\setminus i}(t-1)\}$ and the output $o_j = \{n_i(t)\}$, for all samples $j = 1, \cdots, T$ in the time series of length T. The loss function $\mathcal{L}_g(\omega)$ in (10) is applied for training, where ω represents the learning parameters of AHN. As before, the training data must be healthy.

$$\hat{n}_i(t) = g^{(i)}_{AHN}\left(n_{\setminus i}(t), n_{\setminus i}(t-1)\right) \tag{9}$$

$$\mathcal{L}_g(\omega) = \frac{1}{2}\sum_j \left(o_j - g^{(i)}_{AHN}(x_j|\omega)\right)^2 \tag{10}$$

Then, it is possible to identify the sensor failure by comparing the actual and the estimate of the sensor signal of node i. Thus, the sensor node with maximum difference among all the sensor signals represents the sensor failure, as the identification function I expressed in (11).

$$I(t) = \left(\max_i \|n_i(t) - \hat{n}_i(t)\|\right) \cdot H(t) \tag{11}$$

2.2.3. Sensor accommodation module

The next step of the SFDIA system consists of replacing the corrupted sensor signal with a proper value. Assuming that node i failed (i.e., $I(t) = i$), then we propose to use the estimate of the sensor signal of node i to accommodate the value while the sensor failure persists. The accommodation function N_i for node i is presented in (12).

$$N_i(t) = \begin{cases} n_i(t) & I(t) = 0 \\ \hat{n}_i(t) & I(t) = i \end{cases} \tag{12}$$

2.2.4. Online statistics module

Lastly, the SFDIA system needs to keep updated the mean μ and standard deviation σ of the total difference E, such that (8) holds over a set of time steps T_{stats}. Both values μ and σ should be calculated using the values of E in the last T_{stats} time steps when there is no sensor failure. For implementation, the threshold α and the time steps T_{stats} need to be set initially.

2.2.5. Overall workflow

To summarize, we present Algorithm 1 that shows the overall procedure of the SFDIA system of the intelligent climate monitoring.

Data: Signals from the sensor nodes.
Result: Sensor failure detection, identification, and accommodation system using AHN models.

Training Step:
1. Collect healthy data from the sensor nodes (n_i).
2. Build the dataset for training AHN models, which consists of inputs x_j and outputs o_j.
3. Train the AHN models ($f^{(i)}_{AHN}$) with the dataset by minimizing the loss function (5).
4. Compute the sensor models ($\hat{n}_{\setminus}$) using (6).

Inference Step:
while *true* **do**
  Failure Detection Module:
  5. Gather data from sensor nodes (n_i).
  6. Compute the estimate of sensor signals using (6).
  7. Calculate the total difference E using (7).
  8. Compute the failure detection function H using (8).
  if H **then**
    Sensor Identification Module:
    9. Detect the sensor failure I using (11).
    Sensor Accommodation Module:
    10. Replace signal of sensor failure $i = I$ by using the accommodation function N_i from (12).
  else
    Online Statistics Module:
    11. Update the statistics μ and σ of the total difference E.
  end
end

Algorithm 1: SFDIA system for the intelligent climate monitoring.

3. Use cases

This section describes two case scenarios where we implemented our intelligent climate monitoring: a laboratory and a room museum. Data of both scenarios consisted of temperature and humidity measurements acquired from a distributed sensors network.

3.1. Acquisition devices

Twelve BLE temperature and humidity sensors for Xiaomi Mijia model LYWSDCGQ/01ZM were used for data acquisition [36]. The sensor device is shown in Fig. 4. The devices were calibrated in a Metrology Laboratory accredited by the National Accreditation Body of Colombia (Organismo Nacional de Acreditación de Colombia - ONAC).

3.2. Description of the measurement area

The laboratory of Control Systems and Robotics of the Instituto Tecnológico Metropolitano, Medellín-Colombia, has a size of 1350 cm by 620 cm. Nine nodes were distributed inside the laboratory, one sensor is located in the external technical room, and two sensors are located in the external hallway. The distribution of the sensors is shown in Fig. 5.

The museum storage room is used to store the specimens and pieces of the collections that are not on display with controlled temperature and humidity. The room has a size of 1000 cm x 1600 cm full of cabinets for the storage. There are cabinets placed

Fig. 4. Temperature and Humidity Sensor for Xiaomi Mijia.

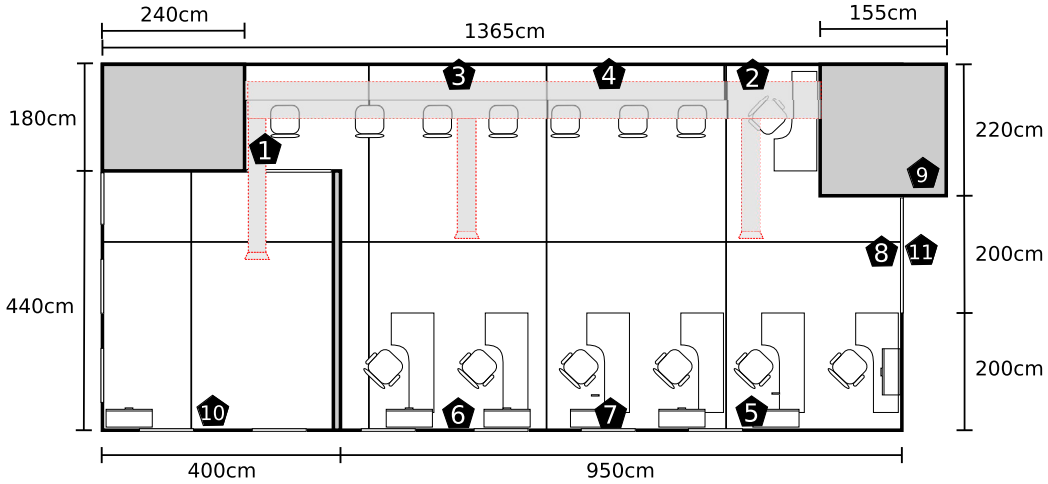

Fig. 5. Distribution of the sensor nodes in the laboratory of Control Systems and Robotics (Scenario 1).

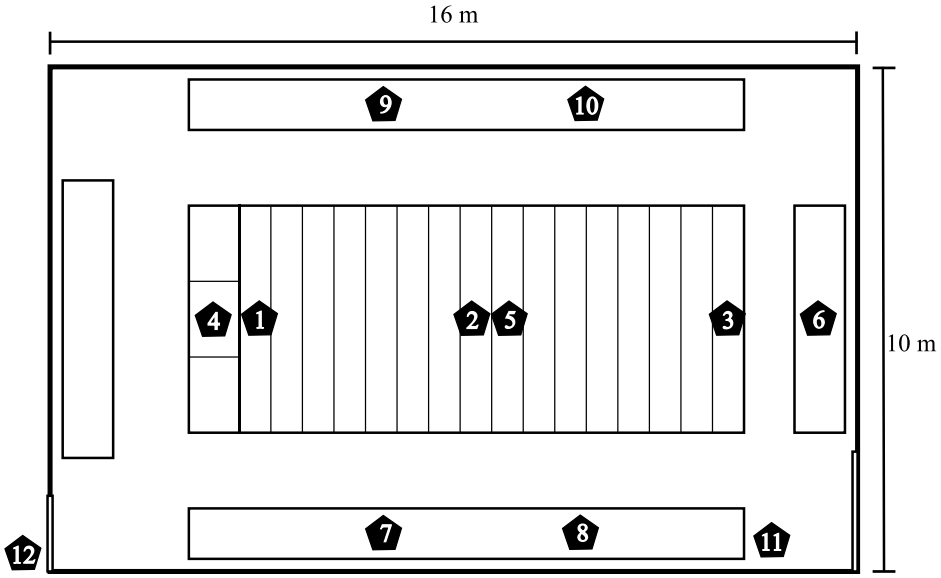

Fig. 6. Distribution of the sensor nodes in the De La Salle Museum of Natural Science. (Scenario 2).

along the walls and a larger one in the center of the room. In the latter, sensors were placed at the top and inside the cabinet (ID 1, 2, 3). The sensor ID 12 was placed outside the room, the sensor ID 11 was located near a humidifier, and the sensors ID 7 and 8 were placed near the air conditioning inlets (see Fig. 6).

Table 1
Scenario 1 – Laboratory: RMSE values for the benchmark of the failure detection module using four machine learning models.

Model	Humidity - training [RH%]	Humidity - testing [RH%]	Temperature - training [ºC]	Temperature - testing [ºC]
AHN	0.65 ± 0.32	**0.87 ± 0.33**	0.21 ± 0.09	**0.25 ± 0.09**
MLP	0.57 ± 0.32	0.92 ± 0.58	0.17 ± 0.06	0.27 ± 0.11
SVM	0.81 ± 0.49	0.96 ± 0.61	0.24 ± 0.11	0.29 ± 0.13
DT	**0.17 ± 0.09**	1.23 ± 0.61	**0.06 ± 0.01**	0.34 ± 0.13

Table 2
Scenario 1 – Laboratory: RMSE values of the twelve nodes for the AHN models in both training and testing sets. The mean and standard deviation of the RMSE values are also shown.

Sensor node	Humidity - training [RH%]	Humidity - testing [RH%]	Temperature - training [ºC]	Temperature - testing [ºC]
1	0.39	0.64	0.12	0.16
2	1.01	1.35	0.34	0.31
3	0.25	0.35	0.09	0.12
4	0.36	0.47	0.11	0.15
5	0.72	1.06	0.31	0.27
6	0.71	0.94	0.25	0.36
7	0.48	0.95	0.18	0.37
8	0.28	0.38	0.10	0.12
9	1.05	0.99	0.28	0.25
10	1.18	1.08	0.27	0.35
11	0.82	1.06	0.25	0.34
12	0.58	1.16	0.21	0.21
mean	0.65	0.87	0.21	0.25
std	0.32	0.33	0.09	0.09

3.3. Dataset description

The dataset contains the indoor temperature and relative humidity information collected during one month with twelve sensors for Xiaomi Mijia at the Laboratory of Control Systems and Robotics, and the De La Salle Museum of Natural Sciences, both of the Instituto Tecnológico Metropolitano, Medellín – Colombia. The data were collected at the laboratory from October 1 to 31, 2019, and at the museum from November 1 to 30, 2019. The dataset consists of a total of 4,164,267 values, organized for each scenario in twelve files in text format that contain the values of the timestamp, relative humidity and temperature separated by commas. Each file contains an average of approximately 58,300 values of each variable. A complete description and access to the database can be found in [37].

4. Experimental results

This section reports the experimental setup and the results obtained using the intelligent climate monitoring system in both scenarios.

4.1. Scenario 1: laboratory

We first built the AHN models ($f_{AHN}^{(i)}$ and $g_{AHN}^{(i)}$) required in the SFDIA system for this scenario with $k = 12$ sensor nodes in the area. For this case scenario, we split the data using the first 21 days (70% of data approximately) for training and the last 10 days (30% of data approximately) for testing. Each AHN model was trained using $m = 5$ molecules and $b = 0.1$ of batch size. We conducted the same procedure for humidity and temperature signals.

Before running the entire experiment, we decided to benchmark our AHN-based failure detection module among using three well-known machine learning models [22,38,39]: multilayered neural networks (MLP), support vector machines (SVM), and decision trees (DT). The comparison comprises the training and testing of the twelve sensor nodes and reporting the mean and standard deviation of the RMSE values. Table 1 summarizes the results of the comparison among the failure detection module using different machine learning models.

From Table 1, we can observe that DT model overfitted, MLP and SVM performed similar results, and AHN model outperformed in testing. We also performed a Wilcoxon test to determine the significance of similarity between AHN and the other models. Results for temperature reported that AHN is statistically similar to MLP and SVM, but DT is not similar ($p_{MLP} = 0.1260$, $p_{SVM} = 0.4357$, $p_{DT} = 0.00003$; with 95% of confidence). Similar results were obtained for humidity ($p_{MLP} = 0.4025$, $p_{SVM} = 0.4705$, $p_{DT} = 0.00009$; with 95% of confidence). In this way, we validated that AHN model is the best choice for this case scenario.

Table 2 summarizes the training and testing evaluation metrics, to say, the root mean square error (RMSE) values for each sensor signal. As noticed, the overall difference between targets and estimates, at the testing dataset, are 0.87 ± 0.33 RH% of humidity and 0.25 ± 0.09 ºC of temperature.

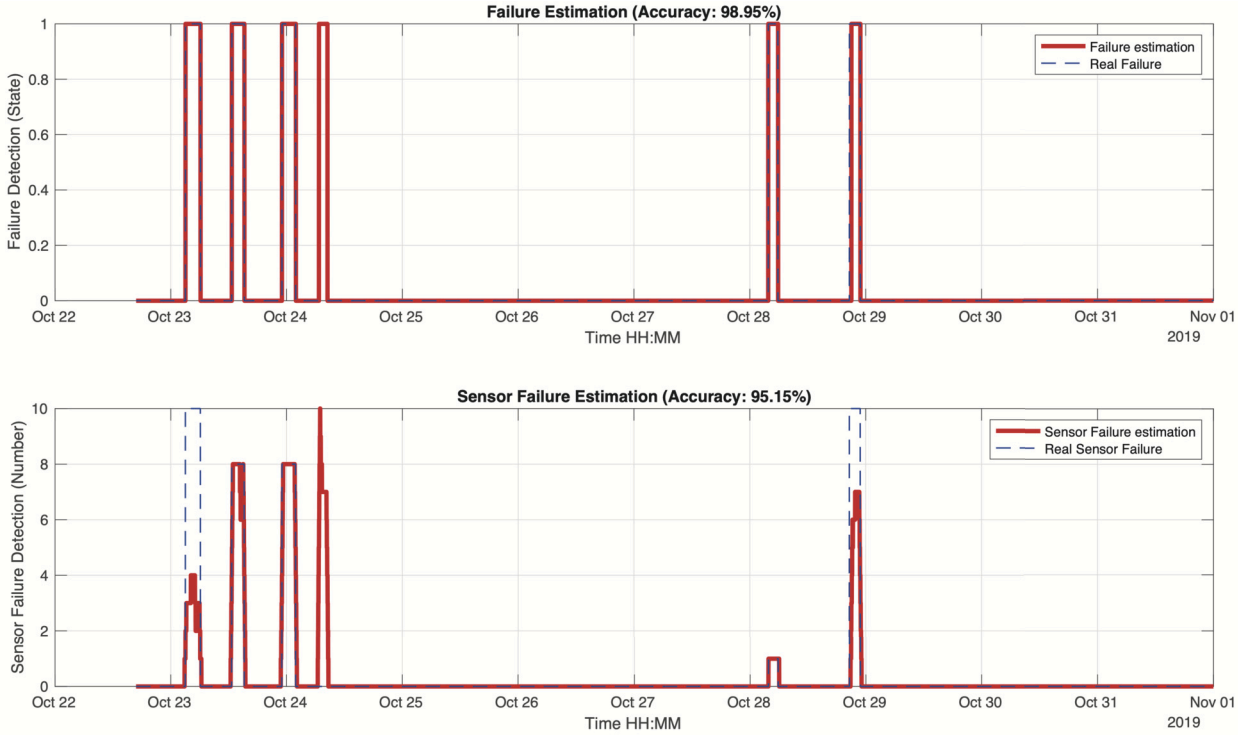

Fig. 7. Scenario 1 – Laboratory: results of the sensor failure detection module (top) and the sensor identification module (bottom), in the humidity testing data.

To validate the intelligent climate monitoring system, we synthetically corrupted the sensor signals with five random failures to the original testing data. The failures consisted of random miscalibrated values in random time windows. For humidity, the relative corrupted values range from −20 to 20 RH%, while for temperature these values range from −10 to 10 ºC. Also, the time window frames vary from 1.5 to 3 hours.

On one hand, the sensor failure detection module of the SFDIA was challenged for finding the failures into the signals, as shown at the top of Fig. 7 and Fig. 8 for humidity and temperature, respectively. We manually set the thresholds and the time steps: $\alpha = 40$ and $T_{stats} = 40$ for humidity, and $\alpha = 10$ and $T_{stats} = 10$ for temperature. It can be seen that this module performed with 98.95% and 99.57% of accuracy in both humidity and temperature data, respectively. On the other hand, we can see the performance of the sensor identification module at the bottom of Fig. 7 and Fig. 8 for humidity and temperature, respectively. As noticed, the sensor identification procedure performed 95.15% and 95.82% of accuracy in humidity and temperature data.

Lastly, Fig. 9 and Fig. 10 show a comparison between the target and the final accommodated sensor signals of humidity and temperature, in testing dataset. Also, Table 3 summarizes the RMSE between the accommodated and the original signals. Specifically, the mean RMSE values are 0.22 ± 0.61 RH% in humidity and 0.08 ± 0.23 ºC in temperature.

4.2. Scenario 2: museum

We trained the AHN models of the SFDIA system for this scenario with $k = 12$ sensor nodes in the museum. Each sensor signal was split in which the first 21 days of data (representing 70% around) were used for training and the remaining 10 days (representing 30% around) of data were used for testing the models. We manually set the hyperparameters of the AHN models as $m = 5$ molecules and $b = 0.1$ of batch size. We repeat this procedure for modeling the humidity and the temperature signals.

Similarly to the previous experiment, we first ran a benchmark of our AHN-based failure detection module among MLP, SVM and DT models. This comparative analysis comprises the training and testing of the twelve sensor nodes and reporting the mean and standard deviation of the RMSE values. Table 4 summarizes the results of this comparison.

From the above, we observe that DT overfitted again, MLP and SVM performed similarly, and AHN outperformed in testing for both humidity and temperature. Then, we performed the Wilcoxon test to determine the significance of similarity between AHN and the other models. Results for temperature reported that AHN and SVM are significantly similar, but AHN differs from MLP and DT ($p_{MLP} = 0.0404$, $p_{SVM} = 0.0885$, $p_{DT} = 0.0001$; with 95% of confidence). The results obtained for humidity showed that AHN is significantly similar to MLP and SVM, but not with DT ($p_{MLP} = 0.2855$, $p_{SVM} = 0.2145$, $p_{DT} = 0.00009$; with 95% of confidence). Lastly, we validated that AHN model is the best choice for this case scenario.

Table 5 summarizes the training and testing RMSE values for each sensor signal. As noticed, the overall difference between targets and estimates are 1.94 ± 1.01 RH% of humidity and 0.29 ± 0.23 ºC of temperature.

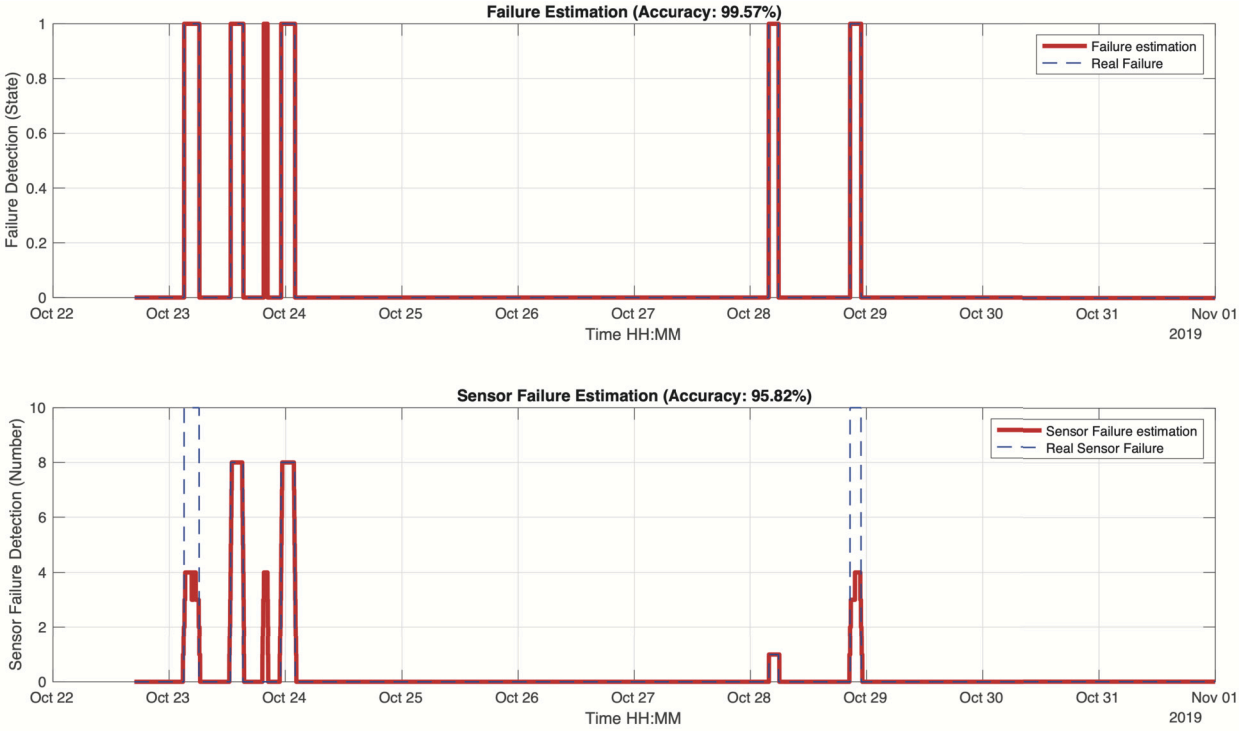

Fig. 8. Scenario 1 – Laboratory: results of the sensor failure detection module (top) and the sensor identification module (bottom), in the temperature testing data.

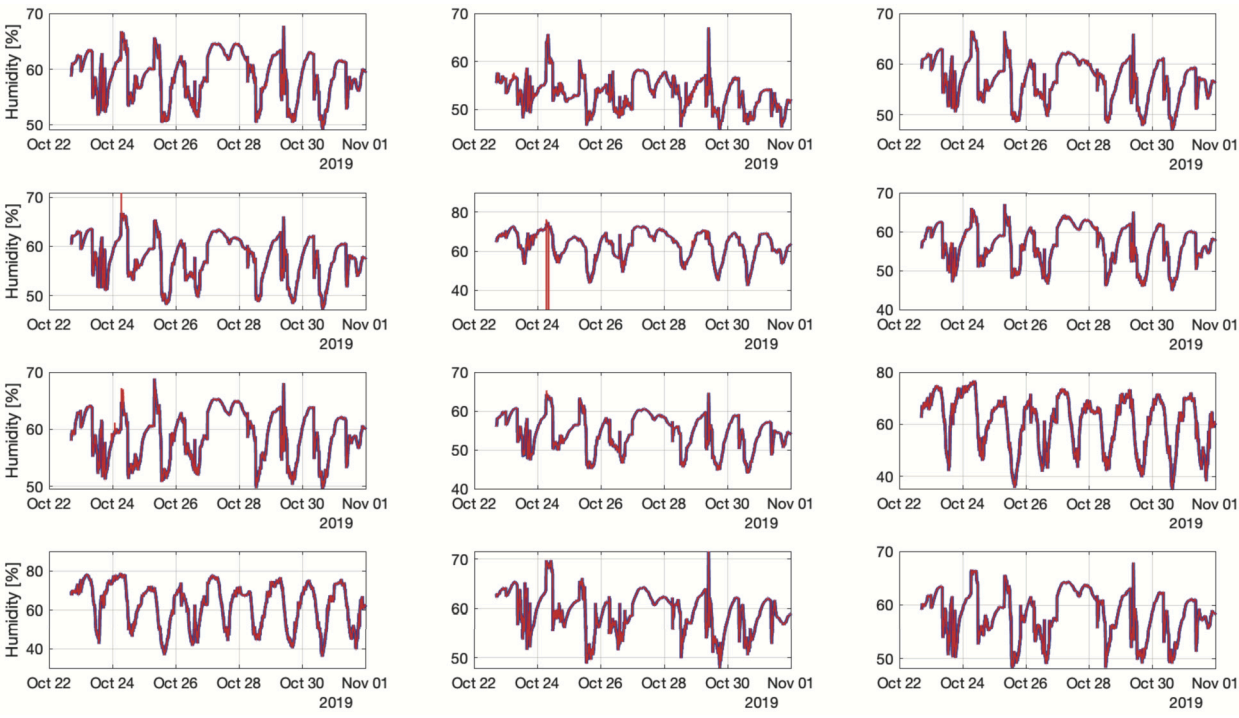

Fig. 9. Scenario 1 – Laboratory: final results between targets (blue line) and accommodation (red line) of humidity sensor signals.

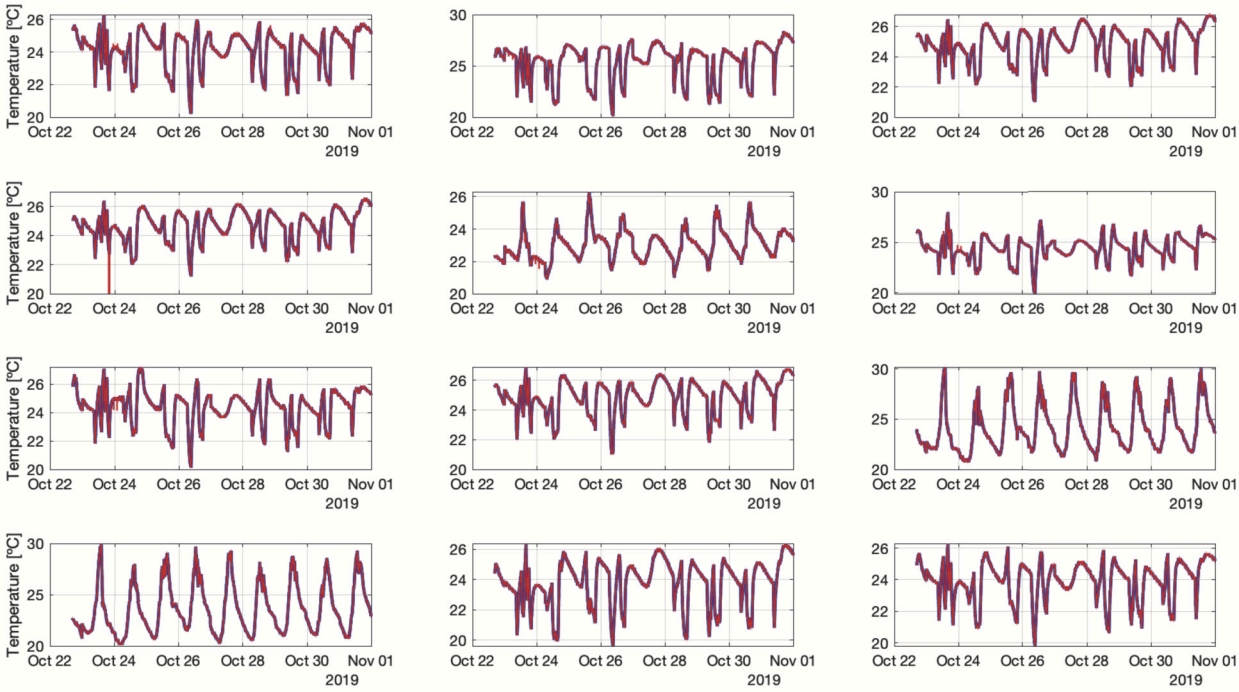

Fig. 10. Scenario 1 – Laboratory: final results between targets (blue line) and accommodation (red line) of temperature sensor signals.

Table 3
Scenario 1 – Laboratory: final results showing RMSE values of the twelve nodes accommodated in testing dataset. The mean and standard deviation of the RMSE values are also shown.

Sensor node	Humidity - testing [RH%]	Temperature - testing [ºC]
1	0.05	0.02
2	0.06	0.02
3	0.02	0.01
4	0.05	0.79
5	2.14	0.02
6	0.08	0.02
7	0.15	0.02
8	0.05	0.02
9	0.01	0.00
10	0.00	0.00
11	0.00	0.00
12	0.00	0.00
mean	0.22	0.08
std	0.61	0.23

Table 4
Scenario 2 – Museum: RMSE values for the benchmark of the failure detection module using four machine learning models.

Model	Humidity - training [RH%]	Humidity - testing [RH%]	Temperature - training [ºC]	Temperature - testing [ºC]
AHN	0.86 ± 0.59	**1.94 ± 1.01**	0.17 ± 0.16	**0.29 ± 0.23**
MLP	0.71 ± 0.42	2.21 ± 1.59	0.13 ± 0.11	0.33 ± 0.27
SVM	1.07 ± 0.87	2.03 ± 1.34	0.22 ± 0.19	0.30 ± 0.25
DT	**0.26 ± 0.12**	2.37 ± 1.51	**0.05 ± 0.02**	0.39 ± 0.31

To validate the intelligent climate monitoring system in this scenario, we added five random failures to the original testing data. It consists of random miscalibrated values in random time windows. For humidity, the miscalibrated values ranges between −20 and 20 RH% in the temperature values ranges between −10 and 10 ºC. The time windows vary from 1.5 to 3 hours.

Table 5
Scenario 2 – Museum: RMSE values of the twelve nodes for the AHN models in both training and testing sets. The mean and standard deviation of the RMSE values are also shown.

Sensor node	Humidity - training [RH%]	Humidity - testing [RH%]	Temperature - training [ºC]	Temperature - testing [ºC]
1	0.53	1.79	0.11	0.18
2	1.14	1.46	0.18	0.26
3	0.90	1.71	0.13	0.27
4	0.82	1.90	0.19	0.29
5	0.45	0.75	0.11	0.13
6	0.53	3.08	0.09	0.22
7	0.55	1.17	0.13	0.15
8	0.69	1.69	0.09	0.17
9	0.99	3.30	0.15	0.61
10	2.56	4.05	0.68	0.88
11	0.46	0.94	0.10	0.13
12	0.68	1.43	0.13	0.14
mean	0.86	1.94	0.17	0.29
std	0.59	1.01	0.16	0.23

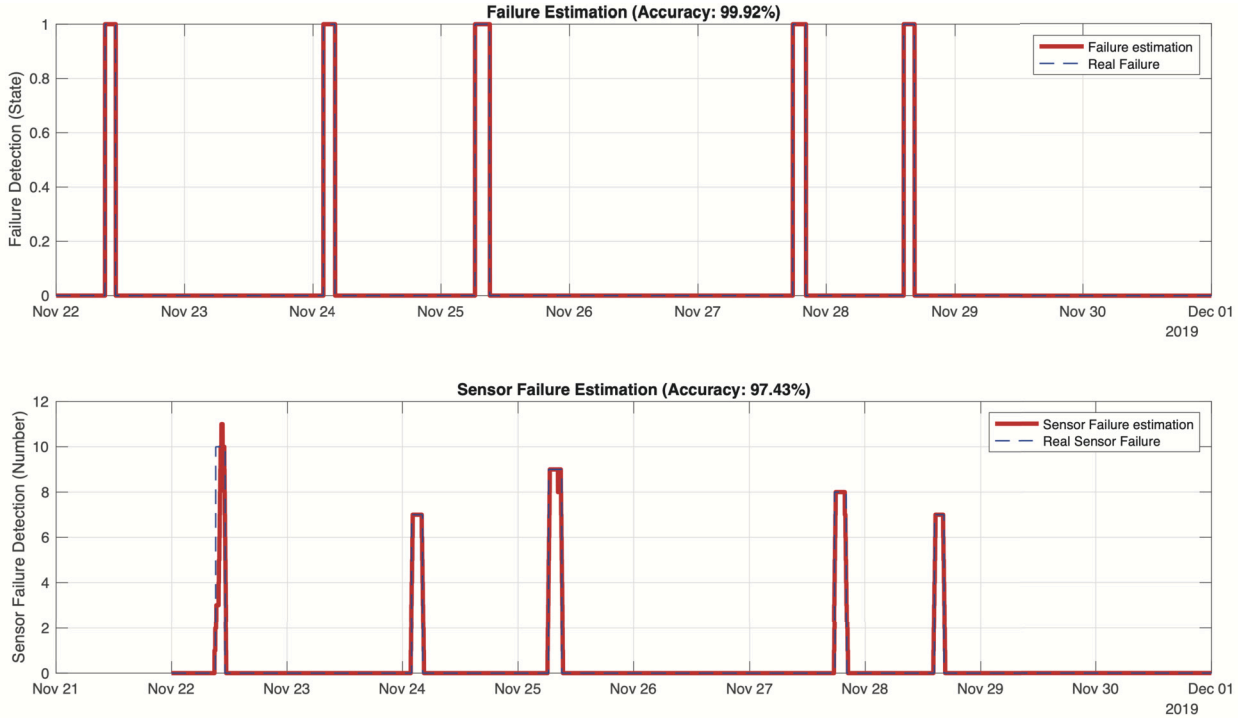

Fig. 11. Scenario 2 – Museum: results of the sensor failure detection module (top) and the sensor identification procedure (bottom) in the humidity testing data.

We manually set the thresholds and the time steps for the SFDIA system: $\alpha = 30$ and $T_{stats} = 30$ for humidity, and $\alpha = 10$ and $T_{stats} = 10$ for temperature. Fig. 11 and Fig. 12 show the sensor failure detection response (top) and the sensor identification response (bottom) for humidity and temperature sensor signals, respectively. As shown, our sensor failure detection module is 99.92% accurate for humidity and 99.44% accurate for temperature. While the sensor identification module obtains 97.43% of accuracy for humidity data and 97.36% of accuracy for temperature.

In addition, Fig. 13 and Fig. 14 show the accommodate sensor signals of both humidity and temperature, in testing dataset. Table 6 summarizes the RMSE between the accommodated and the original signals. The mean RMSE values are 0.13 ± 0.09 RH% in humidity and 0.01 ± 0.01 ºC in temperature.

5. Effects of anomalous data in interpolation analysis

A critical aspect of assessing a system's responsiveness to real-world conditions is verifying its behavior under perturbations. A practical approach involves inducing a controlled perturbation on a sensor within the dataset obtained from the museum and laboratory. In our rigorous methodology, we employ a heat map generated through interpolation of the sensor data. This visualization tool

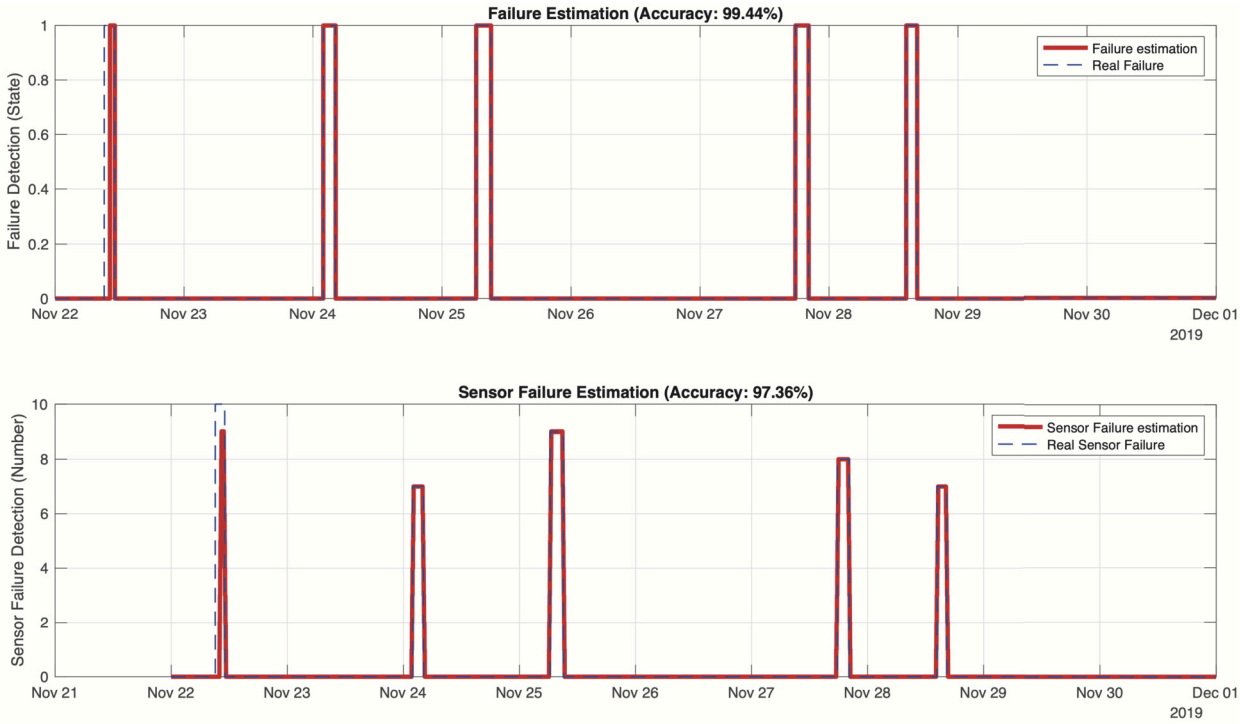

Fig. 12. Scenario 2 – Museum: results of the sensor failure detection module (top) and the sensor identification procedure (bottom) in the temperature testing data.

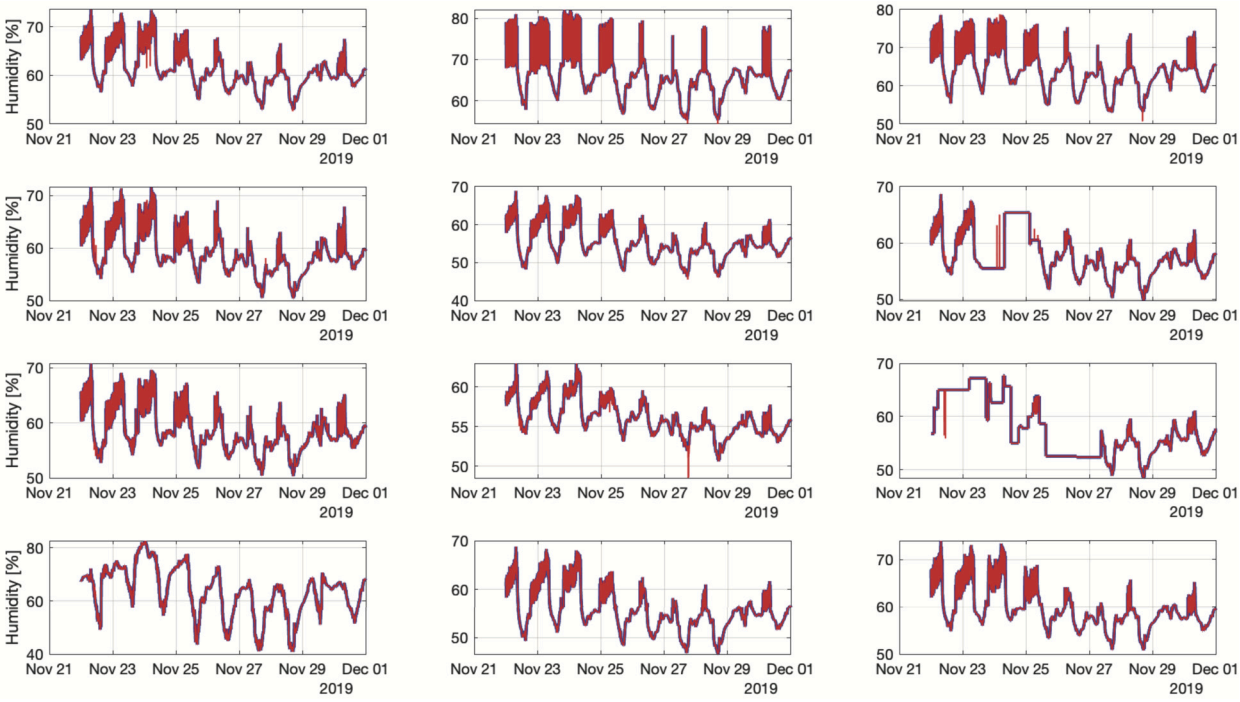

Fig. 13. Scenario 2 – Museum: final results between targets (blue line) and accommodation (red line) of humidity sensor signals.

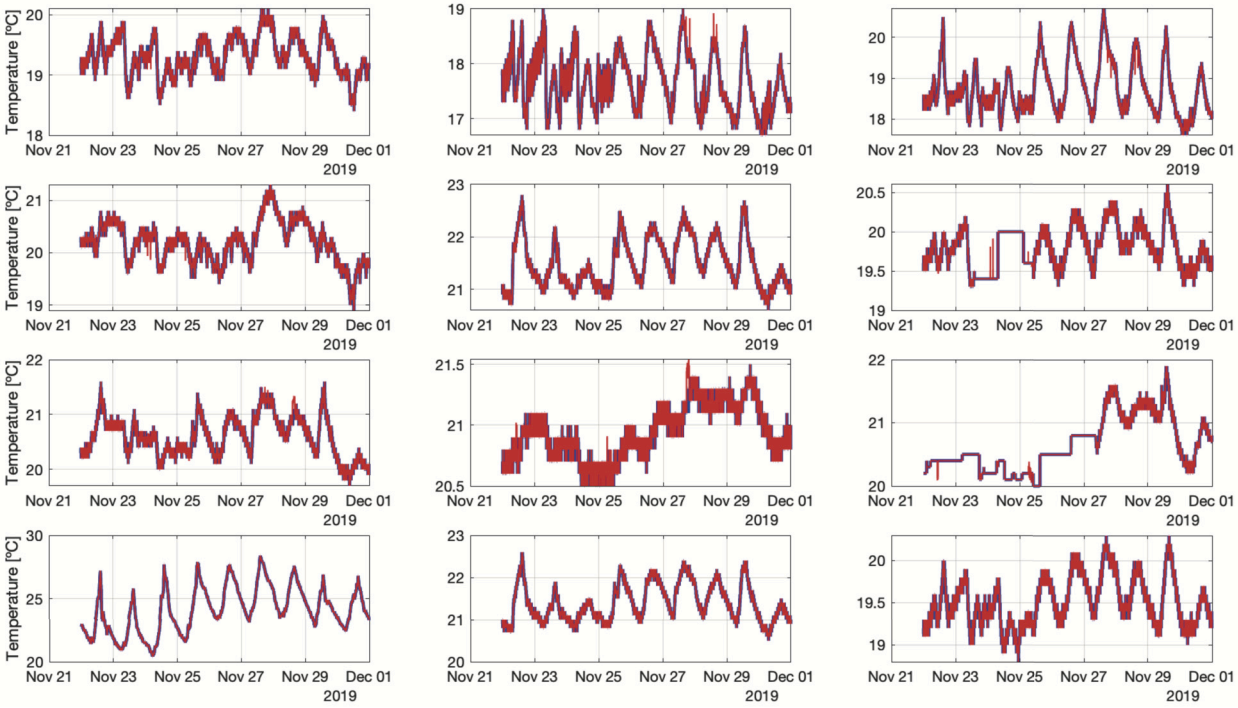

Fig. 14. Scenario 2 – Museum: final results between targets (blue line) and accommodation (red line) of temperature sensor signals.

Table 6
Scenario 2 – Museum: final results showing RMSE values of the twelve nodes accommodated in testing dataset. The mean and standard deviation of the RMSE values are also shown.

Sensor node	Humidity - testing [RH%]	Temperature - testing [ºC]
1	0.14	0.01
2	0.10	0.02
3	0.09	0.02
4	0.12	0.01
5	0.05	0.01
6	0.23	0.01
7	0.12	0.03
8	0.14	0.03
9	0.34	0.01
10	0.16	0.00
11	0.02	0.00
12	0.00	0.00
mean	0.13	0.01
std	0.09	0.01

proves instrumental in comprehending and visualizing the ramifications of sensor failure or abnormality induced by the perturbation. By introducing such deliberate perturbations and analyzing resulting changes in the interpolated heat map, we gain valuable insights into the system's resilience, aiding in verifying responsiveness to varying conditions. The technique allows us to visualize the impact of a singular sensor failure and facilitates a broader understanding of the interplay between sensors and the system as a whole under different operational scenarios.

Figs. 15 and 16 offer a visual representation in the form of a heat map, vividly illustrating the thermal landscape within both the laboratory and museum environments. These comprehensive visuals were meticulously crafted through an interpolation technique, seamlessly integrating the data gathered from the internal sensors meticulously positioned at various strategic points within each site. The result is a holistic depiction of temperature distributions, revealing nuances in the thermal patterns that might otherwise go unnoticed. The color bar thoughtfully accompanying the figures provides an intuitive guide, presenting a spectrum of hues from the cool, calming shades of blue denoting lower temperatures to the warm, vibrant tones of yellow representing the peaks of heat intensity. This gradient enhances the understanding of the temperature range and allows for a quick and insightful analysis of the thermal variations across the spatial expanse of the laboratory and museum.

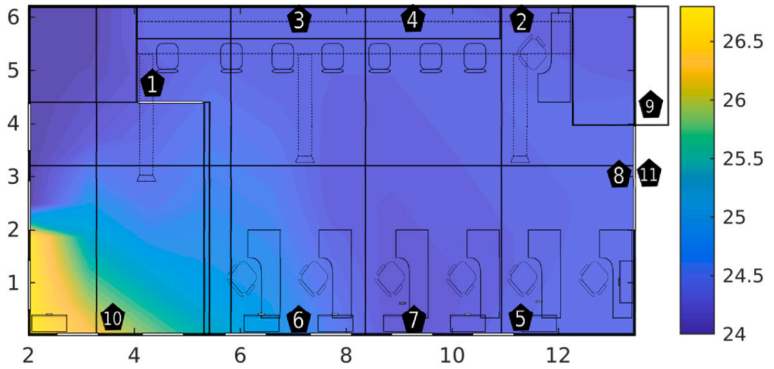

Fig. 15. Heat map of the laboratory using real data and interpolation (Scenario 1).

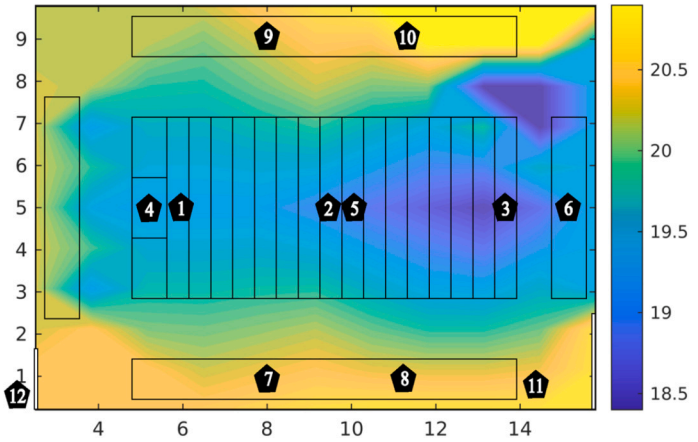

Fig. 16. Heat map of the museum using real data and interpolation (Scenario 2).

Table 7
Data used for the heat map interpolation of the laboratory sensors. Red color represents a disturbance.

Temperature	Sensor number								
	1	2	3	4	5	6	7	8	10
Real [ºC]	24.0	24.3	24.4	24.4	24.5	25.2	24.2	24.5	26.8
Disturbance [ºC]	24.0	24.3	24.4	24.4	24.5	25.2	24.2	16.8	26.8
Accommodation [ºC]	24.0	24.3	24.4	24.4	24.5	25.2	24.2	24.6	26.8

Fig. 17 illustrates a simulated disturbance intentionally introduced to sensor number 8 within the laboratory environment, as outlined in Table 7. The disturbance value for sensor number 8 is shown in red. Sensors 9 and 11 are outside the laboratory and were not considered in generating the heat map. Specifically, we replaced the original value of 24.50 for sensor number 8 with 16.75. The subsequent analysis showcases the system's remarkable ability to accommodate this perturbation, as evidenced in Fig. 18. The system corrects the disturbed measurement, yielding a highly accurate reading of 24.58, representing a mere 0.33 percent error from the original measurement. The experiment exemplifies the system's robustness and precision in swiftly adapting to disturbances and maintaining precise measurements.

Fig. 19 presents an experiment conducted using the museum dataset to evaluate the impact of perturbations on sensor data. The experiment reveals a discernible perturbation effect on a particular sensor, resulting in an error propagation observed within the corresponding heat map. In this study, sensor number 7 was deliberately subjected to perturbation, where the initial value of 20.50 was intentionally altered to 15.13, as outlined in Table 8. After this perturbation, the measurement accommodation mechanism within the system went into effect, rectifying the altered reading and restoring the sensor value to 20.55.

The corrective action showcased a minimal error of a mere 0.24 percent compared to the original measurement, underlining the effectiveness of the accommodation mechanism in mitigating perturbation-induced errors. The experiment provides valuable insights into the robustness and precision of the measurement accommodation process in the context of sensor data disturbances, see Fig. 20.

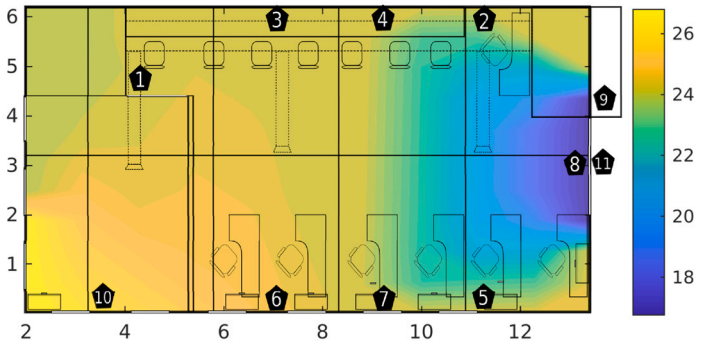

Fig. 17. Heat map of the laboratory when the perturbation is applied in sensor number 8 (Scenario 1).

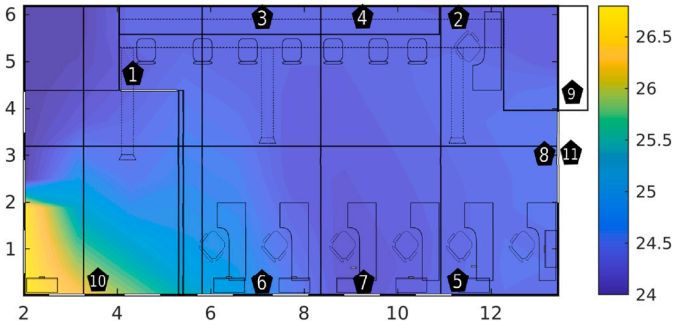

Fig. 18. Heat map of the laboratory after system accommodation (Scenario 1).

Table 8
Data used for the heat map interpolation of the museum sensors. Red color represents a disturbance.

	Sensor number										
	1	2	3	4	5	6	7	8	9	10	11
Real [ºC]	19.3	17.7	18.4	20.3	20.9	19.4	20.5	20.8	20.2	20.9	20.8
Disturbance [ºC]	19.3	17.7	18.4	20.3	20.9	19.4	15.1	20.8	20.2	20.9	20.8
Accommodation [ºC]	19.3	17.7	18.4	20.3	20.9	19.4	20.6	20.8	20.2	20.9	20.8

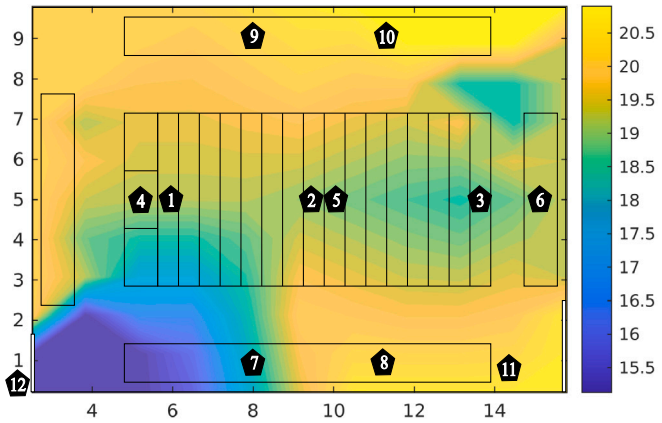

Fig. 19. Heat map of the museum when the perturbation is applied in sensor number 7 (Scenario 2).

6. Discussion

From the above results, it can be seen that the SFDIA system, based on AHN models, is able to both identify potential failures, determine the affected sensor and locate corrupted signals, and replace faulty signals with accurate estimates of climatic variables, thus ensuring the continuity of measurements. In that sense, the proposed system has the following advantages: it operates over a

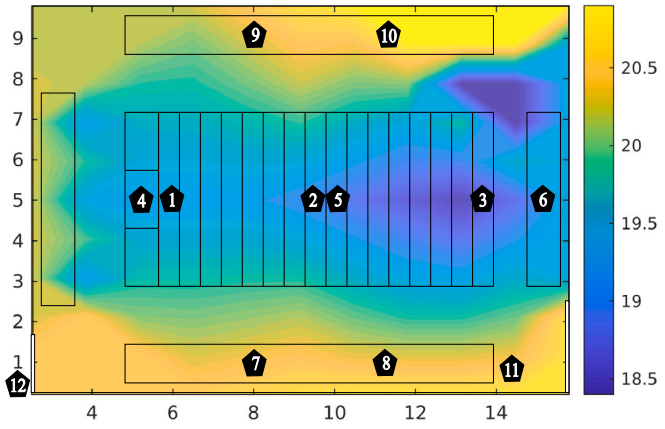

Fig. 20. Heat map of the museum after system accommodation (Scenario 2).

wireless sensor network (WSN) in real-time, ensuring prompt detection and response to sensor failures. The system can detect and identify sensor failures with high accuracy, reaching up to 95% in the experiments conducted. It can accommodate sensor signals with root mean squared errors less than 0.22 RH% in humidity and 0.08 ºC in temperature, indicating high precision. The system is flexible to different measurement variables and can adapt to different numbers of sensor nodes, showcasing its adaptability to various scenarios. Nonetheless, a number of limitations have been identified in the SFDIA system. It needs more data acquisition from sensor nodes to achieve better accuracy in training AHN models, it needs an improved graphical representation of the sensors and their environment, and it also needs to quickly adapt to disturbances and maintain accurate measurements for comfort and preservation analysis.

7. Conclusions

In this work, an intelligent climate monitoring system was developed for humidity and temperature variables in enclosed spaces based on artificial hydrocarbon networks models over a wireless sensor network, where one month of observation was used for each case in two different areas. The experiments were conducted in two scenarios. In the museum storage room scenario, controlled values of temperature and humidity were obtained to ensure the preservation conditions of the objects in a museum. In the second scenario, a laboratory room, which contains multiple workstations, where the staff turns on or off the air conditioning depending on the feeling of comfort, generating an uncontrolled environment for the variables to be obtained. The results showed an accuracy of 95% achieved for the detection of failures and less than 5% error in the estimation of temperature and humidity variables for both spaces.

The analysis of temperature and humidity distributed in controlled environments using methods that combine observations and artificial intelligence is important because multiple factors influence the behavior of these variables and it is easier to build models based on observations than to develop simulated models based on effects alone.

Future work considers improving the efficiency of the SFDIA system by capturing relationships between sensor nodes and exploiting graph representations, and increasing the amount of data for training models. In the long term, we consider scaling the intelligent climate monitoring system to take advantage of many other climate and contextual variables indoors, to monitor and control them for creating comfort conditions. It is worth noting to say that this intelligent monitoring system can be adapted to be used in other sensor domains, such as healthcare, surveillance, robotics, and aerospace technologies.

Ethics declarations statement

Review or approval by an ethics committee was not needed for this study because it does not involve human or animal experimentation.

CRediT authorship contribution statement

Hiram Ponce: Writing – original draft, Visualization, Validation, Supervision, Software, Methodology, Investigation, Formal analysis, Conceptualization. **Sebastián Gutiérrez:** Writing – original draft, Validation, Supervision, Resources, Project administration, Methodology, Investigation, Formal analysis, Conceptualization. **Juan Botero-Valencia:** Writing – original draft, Visualization, Supervision, Software, Resources, Methodology, Investigation, Funding acquisition, Formal analysis, Data curation, Conceptualization. **David Marquez-Viloria:** Writing – original draft, Visualization, Validation, Software, Methodology, Formal analysis, Data curation, Conceptualization. **Luis Castano-Londono:** Writing – original draft, Supervision, Software, Resources, Methodology, Investigation, Formal analysis, Data curation, Conceptualization.

Declaration of competing interest

The authors declare the following financial interests/personal relationships which may be considered as potential competing interests: Juan Botero-Valencia reports financial support was provided by Instituto Tecnológico Metropolitano & FLY NORTH SAS with grant numbers P20223 and 70706. If there are other authors, they declare that they have no known competing financial interests or personal relationships that could have appeared to influence the work reported in this paper.

Data availability

Data is not publicly available. Data will be made available on request.

Acknowledgements

This study were supported by the Automática, Electrónica y Ciencias Computacionales (AE&CC) Group COL0053581, at the Sistemas de Control y Robótica Laboratory, attached to the Instituto Tecnológico Metropolitano. This work is part of the project "Intelligent machine vision system with hardware acceleration for industrial IoT applications" with code P20223 and 70706, funded by the Instituto Tecnológico Metropolitano and FLY NORTH SAS.

References

[1] Y. Al horr, M. Arif, M. Katafygiotou, A. Mazroei, A. Kaushik, E. Elsarrag, Impact of indoor environmental quality on occupant well-being and comfort: a review of the literature, Int. J. Sustain. Built Environ. 5 (1) (2016) 1–11, https://doi.org/10.1016/j.ijsbe.2016.03.006.
[2] R. Paolini, et al., The hygrothermal performance of residential buildings at urban and rural sites: sensible and latent energy loads and indoor environmental conditions, Energy Build. (2017), https://doi.org/10.1016/j.enbuild.2016.11.018.
[3] Y. Ma, et al., A review of the impact of outdoor and indoor environmental factors on human health in China, Environ. Sci. Pollut. Res. 27 (34) (2020) 42335–42345, https://doi.org/10.1007/s11356-020-10452-5.
[4] C.J. Simonson, M. Salonvaara, T. Ojanen, The effect of structures on indoor humidity - possibility to improve comfort and perceived air quality, Indoor Air (2002), https://doi.org/10.1034/j.1600-0668.2002.01128.x.
[5] Yanxiao Feng, Shichao Liu, Julian Wang, Jing Yang, Ying-Ling Jao, Nan Wang, Data-driven personal thermal comfort prediction: a literature review, Renew. Sustain. Energy Rev. 161 (2022) 112357, https://doi.org/10.1016/j.rser.2022.112357.
[6] Jiazhen Ling, Daniel A. Dalgo, Shengwei Zhu, Yiyuan Qiao, Lingzhe Wang, Vikrant Aute, Jelena Srebric, Jan Muehlbauer, Yunho Hwang, Reinhard Radermacher, Energy savings and thermal comfort evaluation of a novel personal conditioning device, Energy Build. 241 (2021), https://doi.org/10.1016/j.enbuild.2021.110917.
[7] Wooyoung Jung, Farrokh Jazizadeh, Energy saving potentials of integrating personal thermal comfort models for control of building systems: comprehensive quantification through combinatorial consideration of influential parameters, Appl. Energy 268 (2020), https://doi.org/10.1016/j.apenergy.2020.114882.
[8] S. Kim, J. Ryu, W.-H. Hong, Classification of thermal environment control indicators according to the thermal sensitivity of office occupants, Heliyon 10 (4) (2024) e26038, https://doi.org/10.1016/j.heliyon.2024.e26038.
[9] F. Stazi, B. Gregorini, A. Gianangeli, G. Bernardini, E. Quagliarini, Design of a smart system for indoor climate control in historic underground built environment, https://doi.org/10.1016/j.egypro.2017.09.558, 2017.
[10] Bin Yang, Xiaojing Li, Yihang Liu, Lingge Chen, Ruiqi Guo, Faming Wang, Ke Yan, Comparison of models for predicting winter individual thermal comfort based on machine learning algorithms, Build. Environ. 215 (2022), https://doi.org/10.1016/j.buildenv.2022.108970.
[11] Usman Ali, Sobia Bano, Mohammad Haris Shamsi, Divyanshu Sood, Cathal Hoare, Wangda Zuo, Neil Hewitt, James O'Donnell, Urban building energy performance prediction and retrofit analysis using data-driven machine learning approach, Energy Build. 303 (2024) 113768.
[12] D. Szagri, B. Dobszay, B. Nagy, Z. Szalay, Wireless temperature, relative humidity and occupancy monitoring system for investigating overheating in buildings, Sensors 22 (22) (2022) 8638, https://doi.org/10.3390/s22228638.
[13] J. Kim, S. Kim, S. Bae, M. Kim, Y. Cho, K.I. Lee, Indoor environment monitoring system tested in a living lab, Build. Environ. 214 (2022) 108879, https://doi.org/10.1016/j.buildenv.2022.108879.
[14] Jagriti Saini, Maitreyee Dutta, Gonçalo Marques, Indoor air quality monitoring systems based on Internet of things: a systematic review, Int. J. Environ. Res. Public Health 17 (14) (2020) 4942, https://doi.org/10.3390/ijerph17144942.
[15] V. Barot, V. Kapadia, Air quality monitoring systems using IoT: a review, in: 2020 International Conference on Computational Performance Evaluation (ComPE), Shillong, India, 2020, pp. 226–231.
[16] M.S. Hadj Sassi, L. Chaari Fourati, Comprehensive survey on air quality monitoring systems based on emerging computing and communication technologies, Comput. Netw. 209 (2022) 108904, https://doi.org/10.1016/j.comnet.2022.108904.
[17] J. Loy-Benitez, S.K. Heo, C.K. Yoo, Imputing missing indoor air quality data via variational convolutional autoencoders: implications for ventilation management of subway metro systems, Build. Environ. 182 (o) (July 2020) 107135, https://doi.org/10.1016/j.buildenv.2020.107135.
[18] B.W. Mersha, H. Ma, Data-driven model for accommodation of faulty angle of attack sensor measurements in fixed winged aircraft, Eng. Appl. Artif. Intell. 111 (o) (March 2022) 104799, https://doi.org/10.1016/j.engappai.2022.104799.
[19] X. Zhang, R. Yang, G. Guo, J. Zhang, Sensor Failure Detection Based on Programmable Switch and Machine Learning, vol. 12737, LNCS. Springer International Publishing, 2021.
[20] Z. Zhang, A. Mehmood, L. Shu, Z. Huo, Y. Zhang, M. Mukherjee, A survey on fault diagnosis in wireless sensor networks, IEEE Access 6 (2018) 11349–11364, https://doi.org/10.1109/ACCESS.2018.2794519.
[21] C.G. Mattera, J. Quevedo, T. Escobet, H.R. Shaker, M. Jradi, Fault detection and diagnostics in ventilation units using linear regression virtual sensors, in: 2018 International Symposium on Advanced Electrical and Communication Technologies (ISAECT), Rabat, Morocco, 2018, pp. 1–6.
[22] H. Darvishi, D. Ciuonzo, E.R. Eide, P.S. Rossi, Sensor-fault detection, isolation and accommodation for digital twins via modular data-driven architecture, IEEE Sens. J. 21 (4) (2021) 4827–4838, https://doi.org/10.1109/JSEN.2020.3029459.
[23] Dominik Martin, Niklas Kühl, Gerhard Satzger, Virtual sensors, Bus. Inf. Syst. Eng. 63 (3) (2021) 315–323.
[24] E. El Rachkidi, N. Agoulmine, N. Chendeb, D. Belaid, Resources optimization and efficient distribution of shared virtual sensors in sensor-cloud, in: 2017 IEEE International Conference on Communications (ICC), Paris, France, 2017, pp. 1–6.
[25] L. Nie, Y. Ren, R. Wu, M. Tan, Sensor fault diagnosis, isolation, and accommodation for heating, ventilating, and air conditioning systems based on soft sensor, Actuators 12 (10) (2023) 389, https://doi.org/10.3390/act12100389.

[26] Ihab Samy, Ian Postlethwaite, Da-Wei Gu, SFDIA of consecutive sensor faults using neural networks–demonstrated on a UAV, Int. J. Control 83 (11) (2010) 2308–2327, https://doi.org/10.1080/00207179.2010.520031.
[27] S.-H. Kwon, H.-S. Ahn, Sensor failure detection, identification and accommodation using neural network and fuzzy voter, in: 2017 17th International Conference on Control, Automation and Systems (ICCAS), Jeju, Korea (South), 2017, pp. 139–144.
[28] H. Ponce-Espinosa, P. Ponce-Cruz, A. Molina, Artificial Hydrocarbon Networks. In: Artificial Organic Networks, Studies in Computational Intelligence, vol. 521, Springer, Cham, 2014.
[29] P. Ponce, H. Ponce, A. Molina, Doubly fed induction generator (DFIG) wind turbine controlled by artificial organic networks, Soft Comput. 22 (2018) 2867–2879, https://doi.org/10.1007/s00500-017-2537-3.
[30] H. Ponce, M. Acevedo, N. Esparza-Duran, A hybrid fuzzy-molecular controller enhanced with evolutionary algorithms: a case study in a one-leg mechanism, J. Franklin Inst. 356 (16) (2019) 9432–9450, https://doi.org/10.1016/j.jfranklin.2019.09.001.
[31] H. Ponce, L. Martínez-Villaseñor, L. Miralles-Pechuán, A novel wearable sensor-based human activity recognition approach using artificial hydrocarbon networks, Sensors 16 (7) (2016) 1033, https://doi.org/10.3390/s16071033.
[32] H. Ponce, P. Ponce, A. Molina, Adaptive noise filtering based on artificial hydrocarbon networks: an application to audio signals, Expert Syst. Appl. 41 (14) (2014) 6512–6523, https://doi.org/10.1016/j.eswa.2013.12.040.
[33] J. Brieva, H. Ponce, E. Moya-Albor, Non-contact breathing rate estimation using machine learning with an optimized architecture, Mathematics 11 (3) (2023) 645, https://doi.org/10.3390/math11030645.
[34] L. Martínez-Villaseñor, H. Ponce, A. Martínez-Velasco, L. Miralles-Pechuán, An explainable tool to support age-related macular degeneration diagnosis, in: 2022 International Joint Conference on Neural Networks (IJCNN), Padua, Italy, 2022, pp. 1–8.
[35] H. Ponce, P.V. de Campos Souza, A.J. Guimaraes, G. Gonzalez-Mora, Stochastic parallel extreme artificial hydrocarbon networks: an implementation for fast and robust supervised machine learning in high-dimensional data, Eng. Appl. Artif. Intell. 89 (2020) 103427, https://doi.org/10.1016/j.engappai.2019.103427.
[36] Temperature and Humidity Sensor for Xiaomi Mijia. Home Assistant, 202, https://www.home-assistant.io/integrations/mitemp_bt/. (Accessed 23 March 2022).
[37] J. Botero-Valencia, L. Castano-Londono, Marquez-Viloria, D. Indoor, Temperature and Relative Humidity Dataset of Controlled and Uncontrolled Environments, vol. 7, Data, 2022, p. 81.
[38] A. Bhattacharjee, A.K. Mondal, A. Verma, S. Mishra, T.K. Saha, Deep latent space clustering for detection of stealthy false data injection attacks against AC state estimation in power systems, IEEE Trans. Smart Grid 14 (2022) 3, https://doi.org/10.1109/TSG.2022.3216625.
[39] M. Ashrafuzzaman, S. Das, A.A. Jillepalli, Y. Chakhchoukh, F.T. Sheldon, Elliptic envelope based detection of stealthy false data injection attacks in smart grid control systems, in: 2020 IEEE Symposium Series on Computational Intelligence (SSCI), 2020.